



저작자표시-비영리-변경금지 2.0 대한민국

이용자는 아래의 조건을 따르는 경우에 한하여 자유롭게

- 이 저작물을 복제, 배포, 전송, 전시, 공연 및 방송할 수 있습니다.

다음과 같은 조건을 따라야 합니다:



저작자표시. 귀하는 원저작자를 표시하여야 합니다.



비영리. 귀하는 이 저작물을 영리 목적으로 이용할 수 없습니다.



변경금지. 귀하는 이 저작물을 개작, 변형 또는 가공할 수 없습니다.

- 귀하는, 이 저작물의 재이용이나 배포의 경우, 이 저작물에 적용된 이용허락조건을 명확하게 나타내어야 합니다.
- 저작권자로부터 별도의 허가를 받으면 이러한 조건들은 적용되지 않습니다.

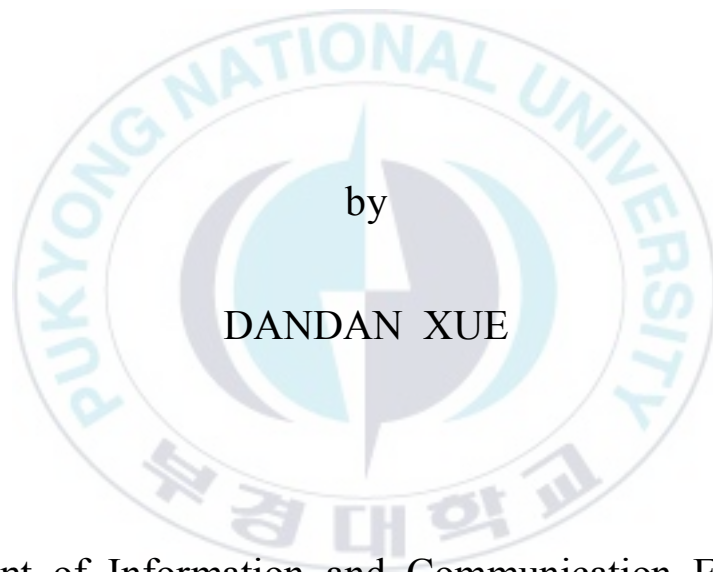
저작권법에 따른 이용자의 권리는 위의 내용에 의하여 영향을 받지 않습니다.

이것은 [이용허락규약\(Legal Code\)](#)을 이해하기 쉽게 요약한 것입니다.

[Disclaimer](#)

Thesis for the Degree of Master of Engineering

Impact of Very Shallow Underwater Channel on Performance of MFSK System



by

DANDAN XUE

Department of Information and Communication Engineering

The Graduate School

Pukyong National University

August 2015

Impact of Very Shallow Underwater Channel on Performance of MFSK System

(극 천해 채널이 MFSK 시스템의 성능에
미치는 영향)

Advisor: Prof. Jong Rak Yoon

by

DANDAN XUE

A thesis submitted in partial fulfillment of the requirements

for the degree of Master of Engineering

in Department of Information and Communication Engineering

The Graduate School,

Pukyong National University

August 2015

Impact of Very Shallow Underwater Channel on
Performance of MFSK System

A Thesis

by

DANDAN XUE

Approved by:

Chairman Prof. Seok-Tea Kim _____

Member Prof. Kyu-Chil Park _____

Member Prof. Jong-Rak Yoon _____

August 2015

Contents

Abstract

Chapter 1 Introduction	1
Chapter 2 Underwater Acoustic Channel.....	5
2.1 Attenuation and Noise.....	5
2.1.1 Spreading loss.....	5
2.1.2 Absorption loss.....	6
2.1.3 Scattering loss.....	7
2.1.4 Ambient noise.....	8
2.2 Multipath.....	8
2.3 Doppler Effect.....	10
2.4 Time variability.....	11
Chapter 3 Underwater Acoustic System, channel model and characterization.....	13
3.1 MFSK modulation system.....	13
3.2 Underwater acoustic channel model and characterization.....	14
Chapter 4 Experimental procedure.....	19
Chapter 5 Results and discussion.....	26
Chapter 6 Conclusions.....	45
References.....	47

Impact of Very Shallow Underwater Channel on Performance of MFSK System

DANDAN XUE

Department of Information and Communication Engineering, The Graduate School,
Pukyong National University

Abstract

The shallow water underwater acoustic channel can be expressed as a frequency selective fast fading channel due to multipath, sea surface roughness, propagation medium and so on change with time and space. In addition the nature of fading varies as communication frequency change for a given channel environment. Therefore the nature of fading changes with time, space, and frequency. The receiving signal amplitude varies with range from transmitter to receiver and therefore fading statistics also changes. Inherent factor of this fading change is a constructive or destructive interference. In this study, multipath, temporal coherence and fading statistics are analyzed using linear frequency modulation (LFM) and pseudo noise (PN) signals. Based on these results, the performance of non-coherent M-ary frequency-shift-keying (MFSK) system is examined and found

that the underwater acoustic channel fading depends strongly on carrier frequency and transmitter to receiver range if there are strong coherent multipath and scattering.



1. Introduction

Underwater acoustic communication is a technique of sending and receiving message below water. With the development of the society, underwater acoustic communication is a rapidly growing field of research and engineering. Its applications become wider and wider such as remote control in off-shore oil industry, pollution monitoring in environmental system, collection of scientific data recorded at ocean-bottom stations, speech transmission between divers, and mapping of the ocean floor for detection of objects, as well as for the discovery of new resources. The application which once was exclusively military has extended into commercial fields[1].

For underwater acoustic communication, the most challenging task is to combat the complex and volatile environment of underwater channel. It is considered to be the most complex channel among all communication channels. In underwater channel, acoustic waves are the best solution for communicating since the electromagnetic (EM) waves propagated under water will suffer serious losses over a short distance.

In underwater channel, sound propagation is largely determined by transmission loss, noise, multipath, and temporal and spatial variability of the channel. Transmission loss and noise which are the principal factors determine the available bandwidth, range and signal-to-noise ratio. Multipath which is time-varying can cause inter-symbol interference (ISI) in communication. It influences signal

design and processing, and often imposes severe limitations on the system performance. Especially in shallow water, time varying multipath propagation is more important comparing to deep water, the multipath arrivals from various paths will interfere with each other over short time scales and cause constructive and destructive interference in received signals. Moreover, Doppler shift and spread which caused by the transmitter or receiver motion and sea surface fluctuations can lead to incorrect symbol decoding. In addition, multipath fading can make the signal amplitude destructively or constructively fluctuated and relative phase of the signal frequencies to fluctuated non-linearly, which will result in signal spectrum fluctuation. Therefore, underwater acoustic channel is also known as a time-varying multipath fading channel[2].

All of these effects above-mentioned can cause BER increasing, so in the underwater acoustic communication the system must be designed to be able to combat the effects of channel environment factors for optimum performance.

The Frequency Shift Keying (FSK) signaling scheme is a non-coherent communication method, because only the symbol energy determines the transmitted signal symbols and phase information is not needed in demodulation. So in theory, FSK is less sensitive to the channel fluctuations and more robust to combat the effects of time-varying shallow water multipath channel. In wireless communication due to high data rate requirement, M-ary modulation has been renewed application. Multiple Frequency Shift Keying

(MFSK) can send multiple bits per transmitted symbol.

There have been many studies for underwater acoustic communication technologies like modulator, equalizer, encoder, OFDM, etc. However, there are only a few studies to research how the time-varying underwater channel affects non-coherent communication systems.

For time varying ocean in water depth of 70 m and a source to receiver range of 3.4 km, the statistics of communication signal amplitude fading considering MFSK underwater acoustic communication has been studied and found that the envelope amplitude statistics shows a non-Rayleigh or a non-Rician distributions[2]. However a Rician distribution has also been found for a direct path and a surface reflected signals[3]. A temporal coherence in shallow water has been studied for three frequency bands of about 1.2, 5, and 22 kHz and focused on the temporal coherence dependency on the signal frequency, the source to receiver range, and the sound velocity profile. It was found that the temporal coherence dependency on frequency and sound velocity profile is different from a theoretical prediction for deep water[4]. The performance of MFSK system was studied to quantify the effects of ocean thermocline variability and the fading signal statistics on the BER[5].

In this paper, MFSK ($M=4$) system was examined in shallow sea. The purpose of this paper is to investigate how the time-varying underwater acoustic multipath fading channel affects the BER of MFSK system and to derive parameters of the optimum system

design in a fading channel. To achieve the purpose, the fading channel's environmental factors on the performance of the MFSK system are analyzed by analysis of channel characteristics such as channel impulse response, temporal coherence and channel coherence bandwidths and fading statistics. Fig. 1 shows the structure of the underwater acoustic communication system.

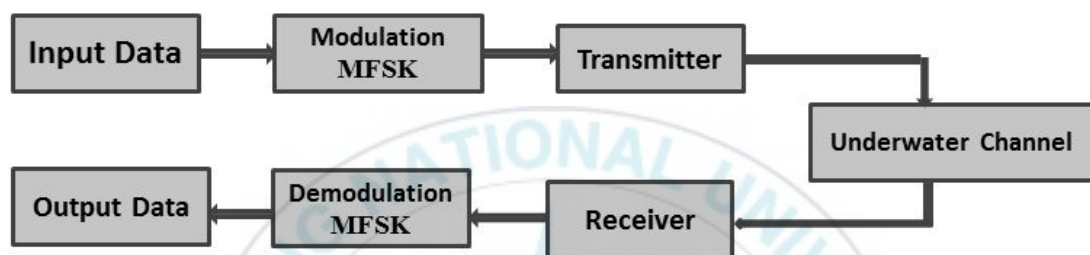


Fig. 1. Structure of the underwater acoustic communication system.

2. Underwater Acoustic Channel

Underwater acoustic communication in general mainly gets affected by the following factors: Channel variations, attenuation and noise, multipath propagation, Doppler shift and spread.

2.1. Attenuation and Noise

In an underwater acoustic channel, the energy of the transmitted signal is partly transferred to heat energy. Some parts of the energy are lost during scattering from the surface, bottom and other objects. In an underwater acoustic channel the loss are considered as spreading loss, absorption loss and scattering loss.

2.1.1 Spreading loss

The spreading loss is often caused by spherical loss for deep water and cylindrical loss for shallow water[6]. For the spherical spreading, the sound wave propagates away from the source uniformly in all directions, the sound levels are therefore constant on spherical surfaces surrounding the sound source and the loss of signal increases with the increase of transmission distance, specifically. It is proportional to square of the distance from source point. When the sound cannot continue to propagate uniformly in all directions and once it reaches the sea surface or sea floor then the sound starts for cylindrical propagation. The cylindrical loss is proportional to inverse

of distance from the source point. Therefore the spreading loss for a distance r from source point is given by

$$L_s = r^k, \quad (1)$$

k is energy spreading factor and it is 2 for spherical, 1 for cylindrical and 1.5 for practical spreading[7].

2.1.2 Absorption loss

In underwater acoustic channel, absorption loss was caused due to the transfer of acoustic energy to the heat energy, which depends on signal's frequency. The absorption loss can be approximated as follows:

$$L_a = a^r, \quad (2)$$

where r is the distance from the source point and a is the frequency dependent term which is given as[7]:

$$a = 10^{a(f)/10}. \quad (3)$$

The term $a(f)$ is the absorption coefficient[8]:

$$a(f) = 0.11 \frac{f^2}{1+f^2} + 44 \frac{f^2}{4100+f^2} + 2.75(10^{-4} f^2) + 0.003. \quad (4)$$

The attenuation coefficient is in dB/km and f is in kHz. The attenuation coefficient based on frequency is shown in Fig.2.

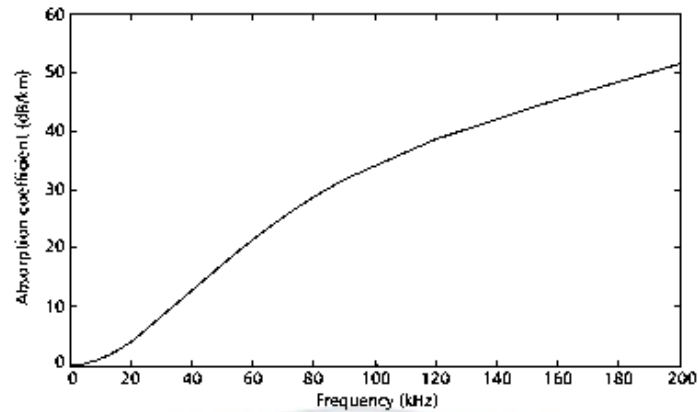


Fig. 2. Absorption coefficient ($10\log(a(f))$) in dB/km).

2.1.3 Scattering loss

The reason for scattering loss is the interaction of sound wave with sea surface and sea floor. If the sea surface and sea floor is rough, most of the sound signal will scatter to the directions which are different from receiver's direction, and cause energy loss in the signal. Besides, there are other two important losses worthy of attention, first is the loss caused by some signals penetrating through the bottom, and another is due that some part of signals does not reflect from the sea surface and passes through the surface. The former signal loss due to penetration into the bottom is greatly higher than absorption through the water. The second loss by surface and bottom scattering increases as grazing angle of the sound increases. In addition, bottom scattering also can cause loss but it greatly depends on the type of the bottom.

2.1.4 Ambient noise

Except losses noise also should be considered in underwater communication system. The noise is closely in relation to frequency and site of underwater channel. There are many noise sources in underwater channel such as turbulence, marine organism, passing ships, rain, winds, breaking waves and man-made noise. All of underwater noise can be classified as ambient noise and site-specific noise. The ambient noise which has a continuous spectrum follows Gaussian statistics and it is not white noise since it is frequency dependent. Nevertheless, site-specific noise often can be said that the nature of noise depends on its source since it has significant non-Gaussian components. Because it is man-made noise, the level of noise in seaside environments is generally higher than the noise in deep or high sea. The amplitude of the total noise can be different from time to time for a certain location and certain frequency due to time variability of the channel environment.

2.2 Multipath

In underwater acoustic communication, multipath is the most important influence factor which is caused by signal reflection at the sea surface, bottom, and any objects, and signal refraction in the water.

Propagation of the acoustic signal occurs over multiple paths, therefore at the receiver side, the received signal is composed of these multi-path signals. Because the received multipath signals can

interfere with each other and the interference is time-varying, the amplitude of the received signal can increase and decrease significantly commonly called multipath fading and the phase of the received signal also changed with time. The variability of the multipath is due to variability of the channel caused by temporal fluctuations such as internal and surface waves, turbulence, tidal flows and platform motion. Particularly the sea surface fluctuation has a serious negative impact on system performance which gives upper and lower side bands in the spectrum of the received sound that duplicates of the spectrum of the sea surface motion. Signal refraction is a consequence of sound speed variation which depends on environmental conditions such as pressure, temperature and salinity. In addition, the number of multi-paths depends on the geometry and physical properties of the channel. Therefore the multipath phenomenon causes distortion in the received signal and the channel impulse response differs from location to location even from time to time for the same location. Fig. 3 shows the multipath formation in shallow (left) and deep water (right).

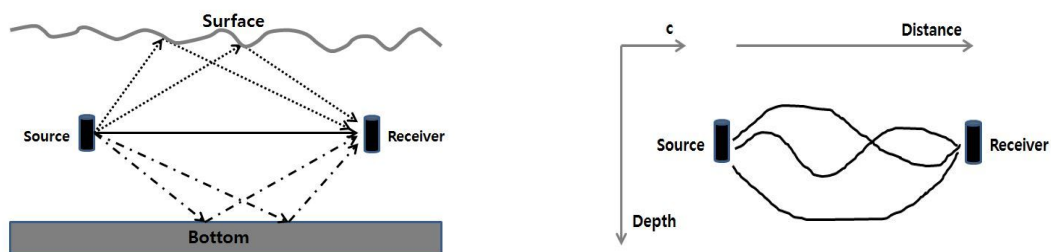


Fig. 3. Multipath formation in shallow (left) and deep water (right).

The channel response can be obtained by adding all responses of multi-paths which have different amplitudes, phase and delays. For a single path the channel response depends on the path length and frequency. In a real underwater channel, there are infinitely multi-paths, but the ones below the noise level can be ignored, only leaving a finite number of significant paths. Each path has its own spreading and multipath delay spread is determined by the longest path or last arrived path.

2.3 Doppler Effect

Relative motion between transmitter and receiver and motion of the platform which transmitter and receiver stay on can cause frequency shifting and frequency spreading which is known as Doppler Effect. The reason is that any change in the path length during propagation of the signal causes expansion (when the path increases) or compression (when the path decreases) of time axis in the received signal[9].

The magnitude of Doppler Effect is proportional to the ratio of relative speed between the transmitter and receiver to the speed of acoustic signal in the channel, that is $a=v/c$ where a is Doppler ratio, v is the relative speed and c is the speed of the acoustic signal. The speed of acoustic wave in underwater channel is low compared to speed of electromagnetic wave and it is comparable to the relative speed between the transmitter and receiver, so it can result in the center frequency of the acoustic signal varied to its left or right side,

which is often called frequency shifting and spreading. Moreover the speed of the platform, which means the speed of waves, currents and tides, is also cannot be ignored comparable to the speed of acoustic signal. Therefore low propagation velocity of the sound in underwater channel can cause severe Doppler distortions. Across the signal bandwidth, each carrier signal may experience a markedly different Doppler shift with time lapse and create non-uniform Doppler distortion.

Doppler effects created by relative motion of the transmitter or receiver can easily be calculated and removed from the received signal. However, Doppler effects created by platform motions cannot easily be calculated or estimated, Therefore the latter makes the Doppler analysis more difficult. Besides, as Doppler effects increase the channel coherence time decreases since the coherence time and Doppler spread are inversely proportional.

2.4 Time variability

There are two main sources of time variability of the underwater channel. The first one is the physical variations of channel and the second is the motion of the transmitter or receiver. The physical variations of channel can also be categorized as long term and short term factors, The former such as daily or monthly changes in thermocline does not affect the instantaneous level of a high frequency communication even if it affects low frequency communication signal. But the latter affects the high frequency

communication signal, such as sea surface boundary fluctuation which effectively causes the displacement of the reflection point by signal reflecting from the time-varying waves. It can result in both scattering of the signal and Doppler spreading due to the changing path length, and lead to signal amplitude, phase and coherence changing[10].



3. Underwater Acoustic System, channel model and characterization

3.1 MFSK modulation system

In order to make the digital signal to transmit in the band pass channel, the digital signal must be modulated to match the characteristics of channels. There are several basic digital modulation methods: ASK, FSK and PSK. In this paper, 4FSK system was applied.

FSK is a frequency modulation scheme in which digital information is transmitted through discrete frequency changes of a carrier signal. MFSK is a variation of FSK that uses more than two frequencies. MFSK is a form of M-ary orthogonal modulation, where each symbol consists of one element from an alphabet of orthogonal waveforms. M, the size of the alphabet, is usually a power of two so that each symbol represents $\log_2 M$ bits[11].

The general analytic expression for MFSK is

$$s_m = \sqrt{\frac{2E_s}{T}} \cos 2\pi(f_c + (m-1)\Delta f)t \quad m=1,2,\dots,M \quad 0 \leq t < T, \quad (5)$$

$$\text{where } \Delta f = f_m - f_{m-1} \text{ with } f_m = f_c + m\Delta f$$

where f_c is the frequency for $m=1$ and $f_c + (m-1)\Delta f$ for the neighboring tones. The amplitude is expressed in terms of the symbol energy E_s . T is symbol time duration. Fig. 4 shows the schematic

diagram of non-coherent MFSK modulation and demodulation.

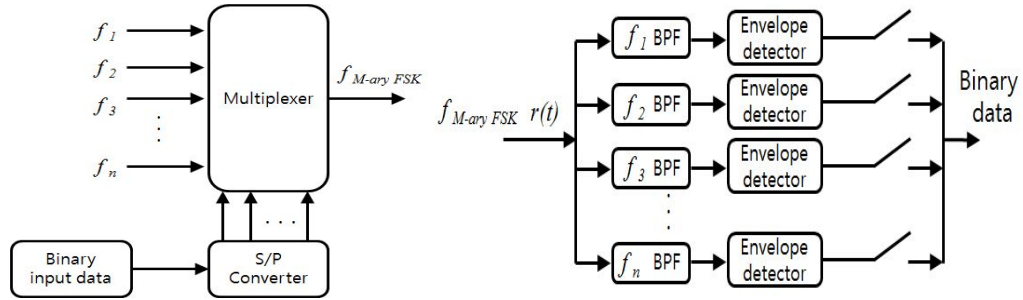


Fig. 4. The schematic diagram of non-coherent MFSK modulation and demodulation.

3.2. Underwater acoustic channel model and characterization.

In this study, the channel governing factors described in chapter 2 are characterized by a channel impulse response, a temporal coherence and a channel coherence bandwidth, and a fading statistics.

Sound signals are scattered and imperfectly reflected by time varying surface. The statistics of the scattered signals are correlated with the statistics of the time varying surface. The scattered sound pressure amplitude will fluctuate and its intensity is the sum of a coherent component without a spatial phase change and an incoherent component with the randomly spatial phase and amplitude changes.

Degree of the surface roughness and magnitude of the coherent component are related to the sea surface coherent reflection coefficient

R_{coh} . A model of the sea surface coherent reflection coefficient R_{coh} at an isotropic Gaussian rough surface is developed and used here without proof[12].

$$R_{coh} = -\exp\{-2(kh\sin\theta)^2\} = -\exp(-2R_{rgh}^2) \quad , \quad (6)$$

here, k , h and θ are the wave number, effective wave height, and a incident-wave grazing angle, respectively. The $kh\sin\theta$ in Eq. (6) is defined as Rayleigh roughness parameter R_{rgh} . The probability density function of the scattered pressure changes from Gaussian to Rayleigh as the R_{rgh} increases. In underwater acoustic communication, the coherent component signal interferes with other coherent signals and the interference level changes and depends on R_{rgh} or R_{coh} . Therefore if the underwater channel is affected by the surface roughness, its impulse response is modeled as the sum of a time invariant coherent multipath components including the coherent component from sea surface and the continuous incoherent scattering components from sea surface.

The equivalent low pass time variant impulse response $h(\tau, t)$ of band pass communication system given as[13]

$$h(\tau, t) = \sum_n \alpha_n(t) e^{-j2\pi f_c \tau_n(t)} \delta(\tau - \tau_n(t)) + \beta(\tau, t) e^{-j2\pi f_c \tau} \quad (7)$$

The first and second terms show discrete and continuous multipath

components, respectively. The $\alpha_n(t)$ is the n th multipath signal's time variable amplitude which depends on time in variant boundary reflection coefficient, propagation path loss, and frequency dependent absorption loss, and $\tau_n(t)$ is the n th multipath time variable delay time. $\beta(\tau, t)$ is a continuous multipath time variable amplitude. Therefore received signal amplitude of band pass system will be faded and the statistics of fading signal envelope $|h(\tau; t)|$ such as Rayleigh or Rice distribution is related to multipath structure.

The autocorrelation function of $h(\tau; t)$ is defined as

$$R_h(\tau_1, \tau_2; \Delta t) = \frac{1}{2} E[h^*(\tau_1; t)h(\tau_2; t + \Delta t)] \quad , \quad (8)$$

where Δt is an observation time difference between two different time instant $h(\tau; t)$. If the observation time difference Δt is set to be 0, then $R_h(\tau_1, \tau_2; 0)$ becomes a multipath intensity profile (MIP). Fourier transform of the autocorrelation function of Δt being set to be 0, give a channel coherence bandwidth B_c . The channel coherence bandwidth B_c in inverse proportion to multipath delay spread is evaluated based on the effective delay-spread τ_s in relations to τ_p in the equation[14]:

$$\tau_s = \sqrt{\overline{t^2} - (\overline{t})^2}. \quad (9)$$

$$\bar{t^2} = \frac{\sum p(t_n) t_n^2}{\sum p(t_n)}, \quad \bar{t} = \frac{\sum p(t_n) t_n}{\sum p(t_n)}. \quad (10)$$

Here, $p(t_n)$ is a power density of a n th path. The relationship between the effective delay spread τ_s , and the channel's coherence bandwidth B_c is given as

$$B_c = \frac{1}{5\tau_s}. \quad (11)$$

If the channel's coherence bandwidth B_c is less than the transmitting signal bandwidth B_s , then it will occur a distortion and error bits. If B_c is greater than the signal bandwidth B_s , the channel is defined as a frequency non selective channel which gives an error-free, stable signal transmission under no channel noise condition.

In time-varying underwater channel, the signal temporal coherence is used to describe the rate of the signal fluctuation depending on Doppler spread effect by boundary or system platform motion. The higher the signal fluctuation, the faster the temporal coherence decreases with time. Temporal coherence is defined by the correlation of the signals separated by a delay time, normalized by the power of the signal, as given by[4]

$$\rho(t, \tau) = \left\langle \frac{[p^*(t) \otimes p(t+\tau)]_{\max}}{\sqrt{[p^*(t) \otimes p(t)]_{\max} [p^*(t+\tau) \otimes p(t+\tau)]_{\max}}} \right\rangle, \quad (12)$$

where $[p^*(t) \otimes p(t)]_{\max}$ means the maximum value of the cross-correlation of the two time series or the convolution of the time-reversed signals (denoted by $*$). A slowly or fast fading channel is defined by large or small coherence time.



4. Experimental procedure

The experiment was conducted in about 15.7 m water depth near Geoje Island in Korea on Aug. 6, 2014. The experimental configuration with typical sea state and parameters are shown in Fig. 5 and Table I, respectively.

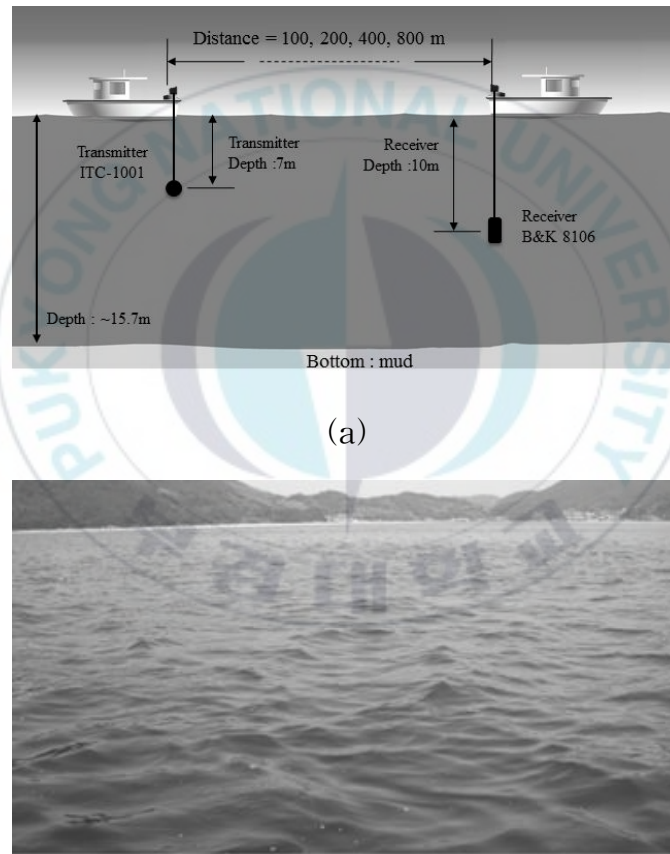


Fig. 5. (a) Experimental configuration and (b) typical sea state.

The ranges between the transmitter and the receiver are set to be

about 100, 200, 400 and 800 m. The depth of receiver and transmitter are set to be 7 and 10 m, respectively. The Lena image of 20,000 bits was transmitted at each transmission range by four different rates which were 200, 400, 800 and 1600 bps. By considering frequency dependent on ambient noise and transmitter output response, 4FSK four-channel system is applied. Each channel transmits 1 of 4 frequencies designated as 0-0, 0-1, 1-0, or 1-1 bits, so there are a total of 16 frequencies in all of four channels as shown in Table II. The orthogonal frequency spacing in each channel are given by $1/T$ (T : symbol period) and all four channel signals are transmitted simultaneously. Therefore symbol rate of each channel is 25 symbols per second (sps) for 200 bps. Guard-bands between channels are inserted by $1/T$. Table II shows orthogonal frequency groups for each data rate. As shown in Table II, the maximum frequency band is from 12 to 19.2 kHz.

Table I. Experimental parameters.

Modulation	4FSK
Channel No.	4
Carrier frequency (kHz)	12-19.2
Symbol rates (sps)	50, 100, 200, 400
Data transmission rates (bps)	200, 400, 800, 1600
Channel guard band	symbol rate
Water depth (m)	~15.7
Bottom property	Mud
Tx and Rx depth (m)	7, 10
Tx and Rx range (m)	100, 200, 400, 800
Information data (bit)	20000
System	Labview

Table II. Orthogonal frequency groups of 4FSK/4Ch for each data rate.

bps/sps		200/50	400/100	800/200	1600/400
Ch1	F1	12000	12000	12000	12000
	F2	12050	12100	12200	12400
	F3	12100	12200	12400	12800
	F4	12150	12300	12600	13200
Ch2	F1	12250	12500	13000	14000
	F2	12300	12600	13200	14400
	F3	12350	12700	13400	14800
	F4	12400	12800	13600	15200
Ch3	F1	12500	13000	14000	16000
	F2	12550	13100	14200	16400
	F3	12600	13200	14400	16800
	F4	12650	13300	14600	17200
Ch4	F1	12750	13500	15000	18000
	F2	12800	13600	15200	18400
	F3	12850	13700	15400	18800
	F4	12900	13800	15600	19200

In actual data transmission, the payload is half of Table I since linear frequency modulation (LFM) and pseudo noise (PN) signals are allocated as shown Fig. 6 which shows a frame structure of a signal. Each frame lasts 1 s. A frame starts with a LFM signal of 10 ms, followed by a 20 ms gap, a 400 ms PN signal, a 20 ms gap and the data signal. LFM signal of 12 to 18 kHz bandwidth was used for the purpose of measuring the channel response. PN signal of 13 to 19 kHz bandwidth was used for symbol synchronization and fading statistics of channel. In actual system, only one of LFM or PN

signals can be used for channel response and symbol synchronization and the payload can be increased.

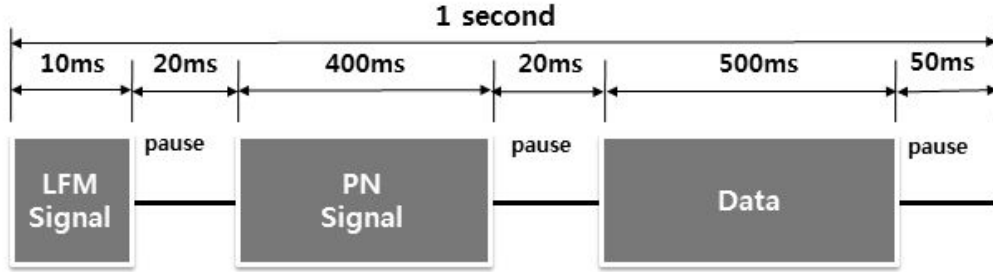


Fig. 6. One frame structure of transmitting signal.

Before data transmission in each range from transmitter to receiver (Tx-Rx range) LFM was also transmitted for 30 s to measure the channel response and temporal coherence. Each LFM signal has 10 ms gap to obtain an independent channel response and temporal coherence with time lapse.

Fig. 7 and 8 show the sound velocity profiles and the eigenray trace results, respectively. In Fig. 8, the numerical value of each eigenray means grazing angle with respect to sea surface plane and only the first five arrivals which could show high signal amplitude are shown. Table III shows the relative time delay (ms) of each eigenray for the four different Tx-Rx ranges.

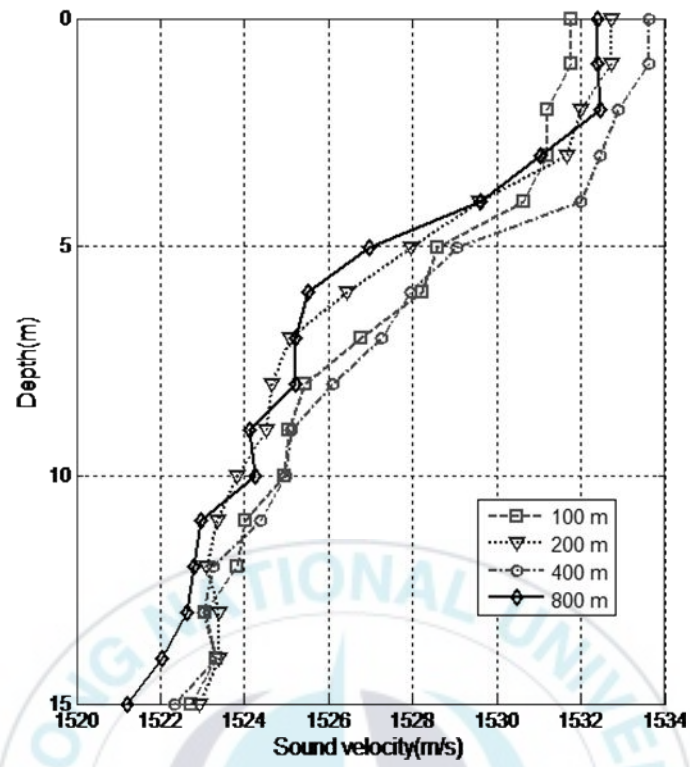
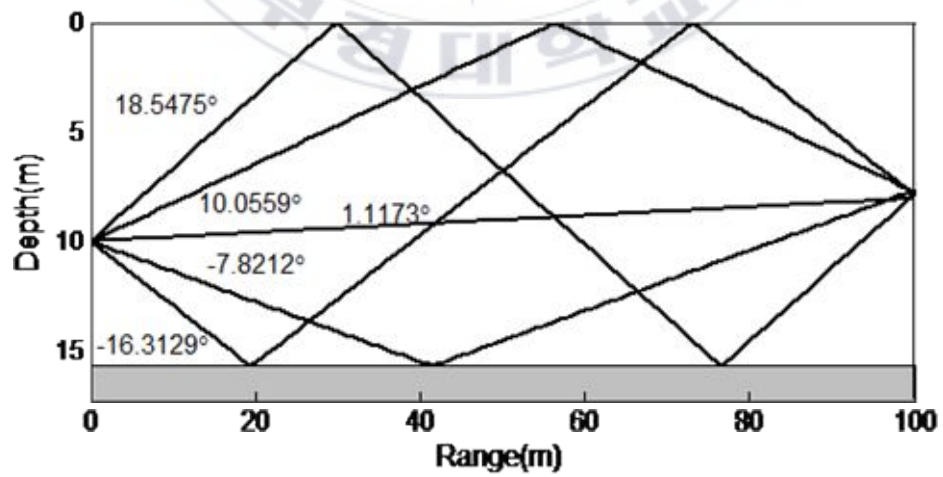
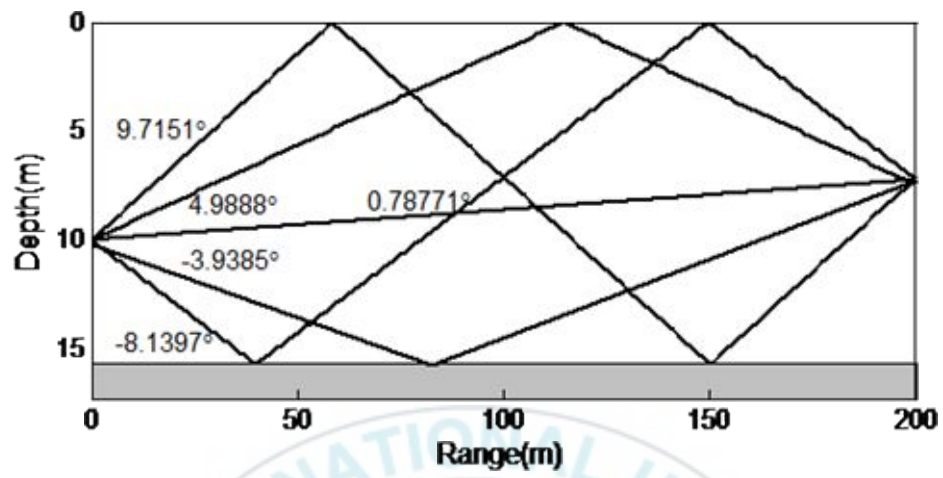


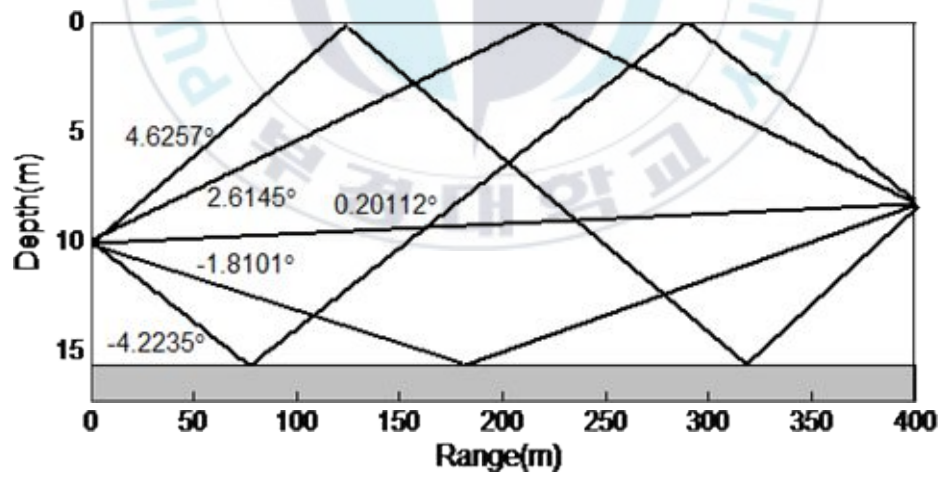
Fig. 7. Sound velocity profiles of experimental site.



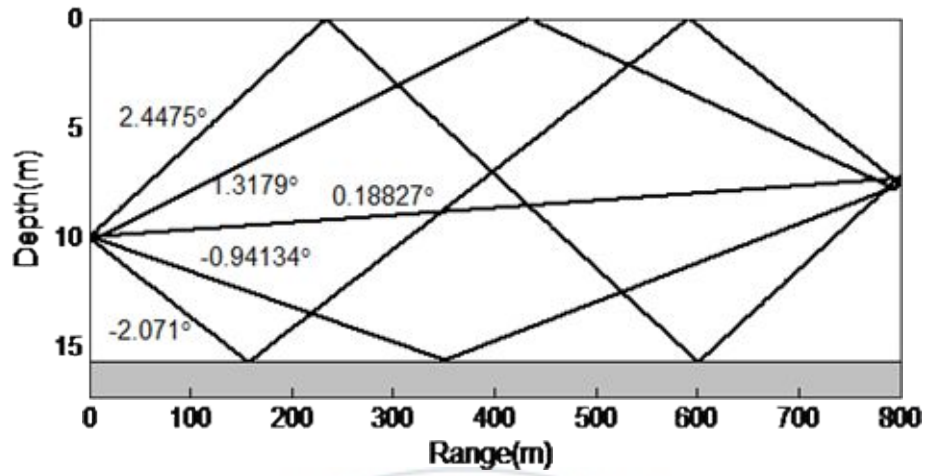
(a)



(b)



(c)



(d)

Fig. 8. Simulated eigenray trace results of four different Tx-Rx ranges: transmitter depth 7 m, and receiver depth 10 m: (a) 100 m; (b) 200 m; (c) 400 m; (d) 800 m.

Table III. Relative time delay (ms) of each eigenray for four different Tx-Rx ranges.

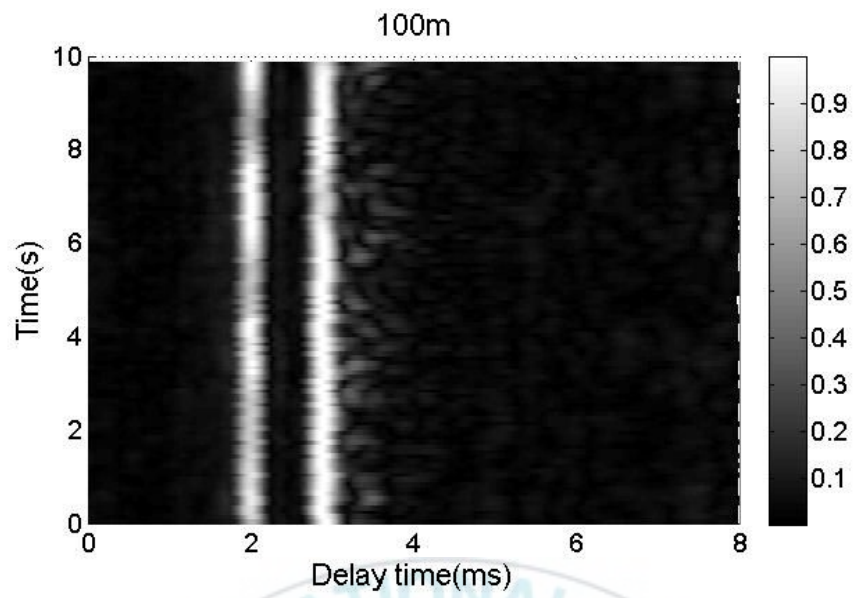
	D	B	S	B-S	S-B
100 m	0	0.60	1.00	2.80	3.60
200 m	0	0.20	0.50	1.30	1.90
400 m	0	0.12	0.28	0.07	0.87
800 m	0	0.07	0.15	0.36	0.48

5. Results and discussion

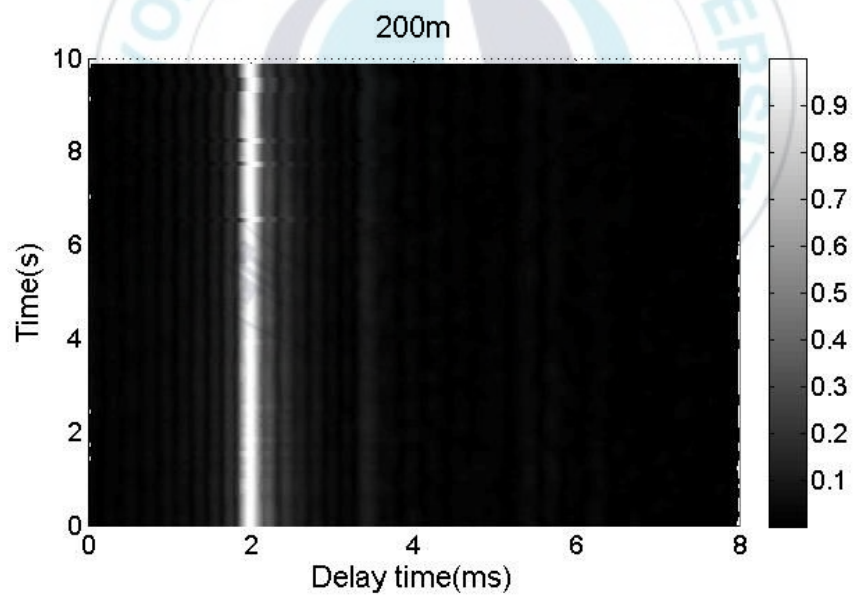
The channel impulse response was analyzed by MIP which is given by matched filtering the received signal with the transmitted signal. LFM signals were used to measure the equivalent low pass channel impulse responses.

Fig. 9 shows the MIPs of 100, 200, 400, and 800 m Tx-Rx ranges. The first strong signals are pretty stable at four ranges. The surface reflected signal is shown clearly in 100 m range but not in other three ranges. The surface reflected signals of other three ranges are lumped together with the direct signal since the time resolution is about 0.2 ms for 6 kHz bandwidth of LFM signal. This is confirmed from each eigenray time delays to direct signal in Table III. Other strong signals in 400 and 800 m range are caused by a bottom reflected signal due to perfect reflection condition for mud bottom.

Average signals of 30 s MIPs in Fig. 9 are Fourier-transformed. Fig. 10 and Table IV show the channel coherence bandwidths of four transmission ranges. The coherence bandwidths will be interpreted in 4FSK BER analysis.



(a)



(b)

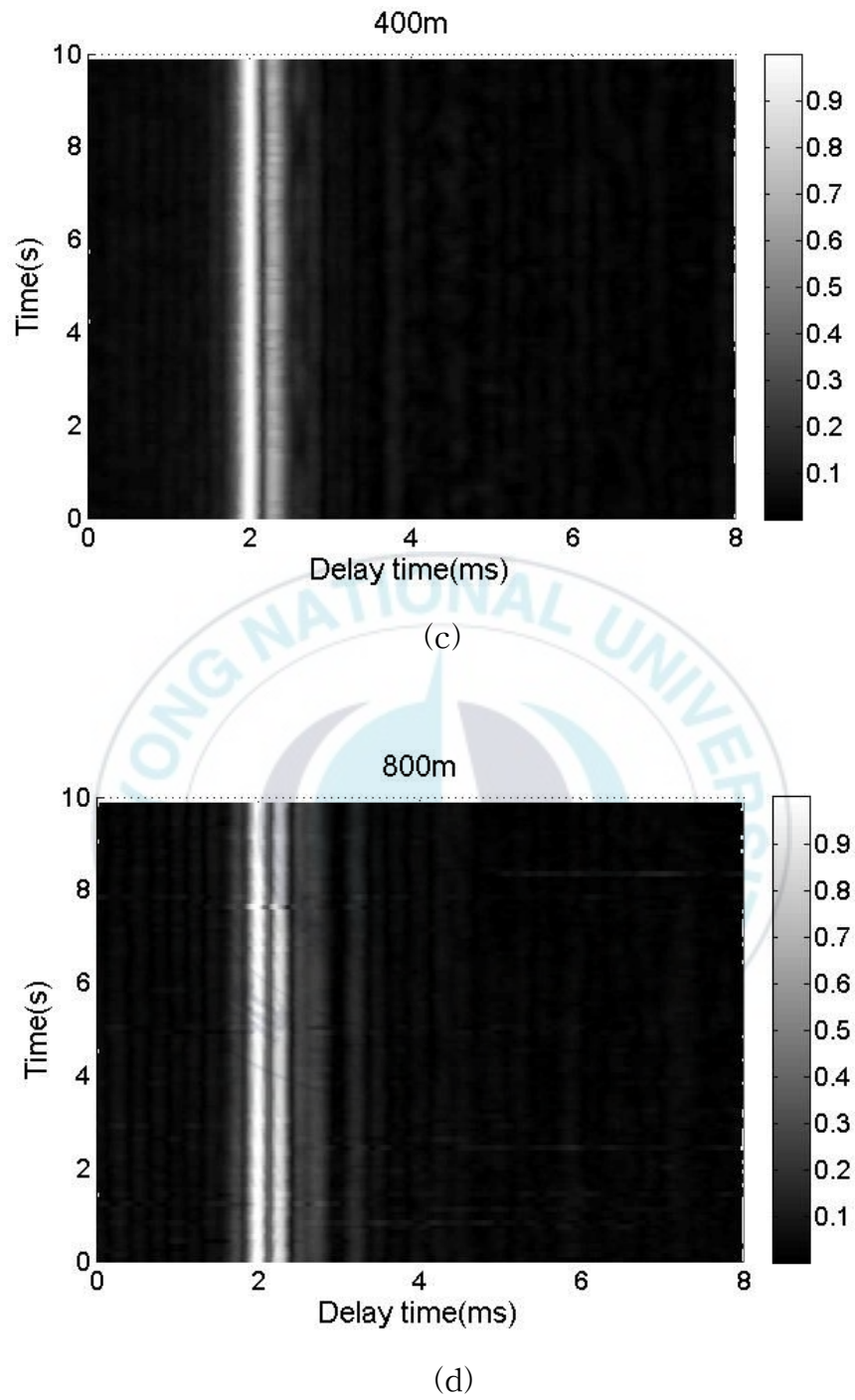
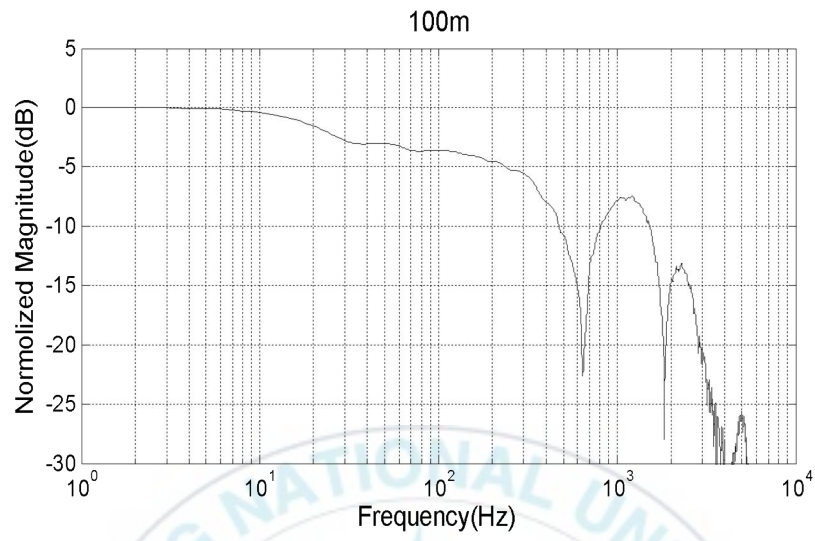
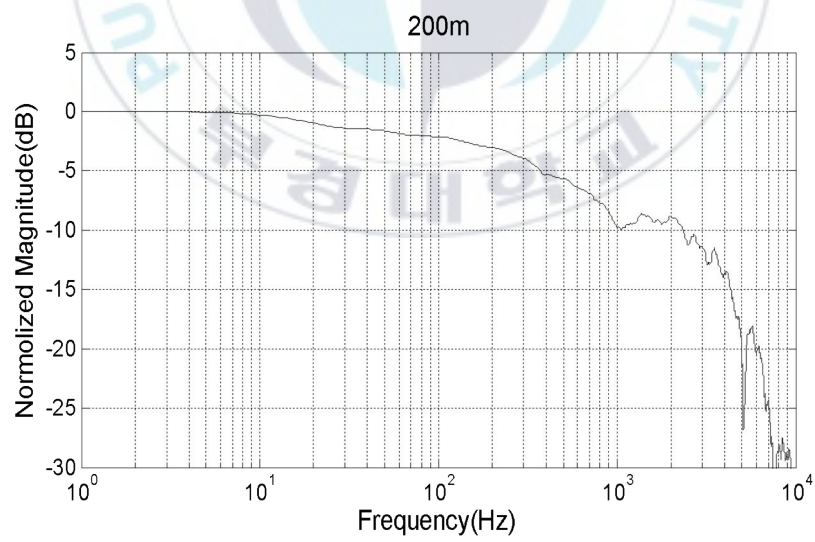


Fig. 9. Measured channel impulse responses as a function of the delay time and geotime: (a) 100 m; (b) 200 m; (c) 400 m; (d) 800 m.



(a)



(b)

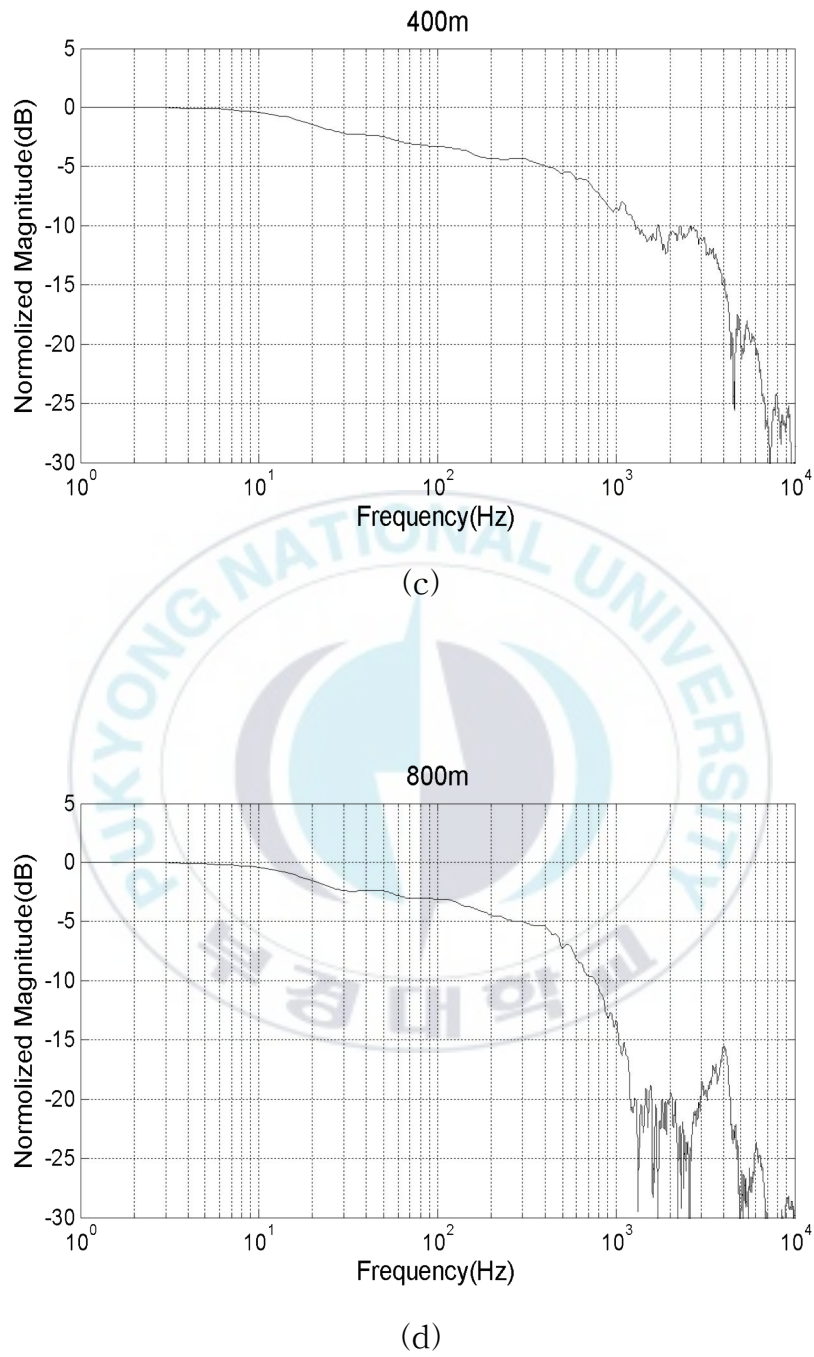
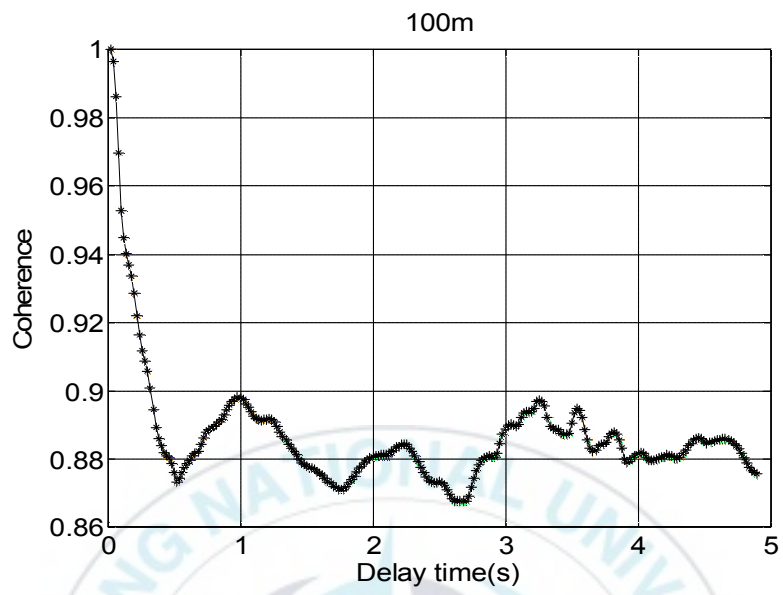


Fig. 10. Channel coherence bandwidths for four Tx-Rx ranges:
(a) 100 m; (b) 200 m; (c) 400 m; (d) 800 m.

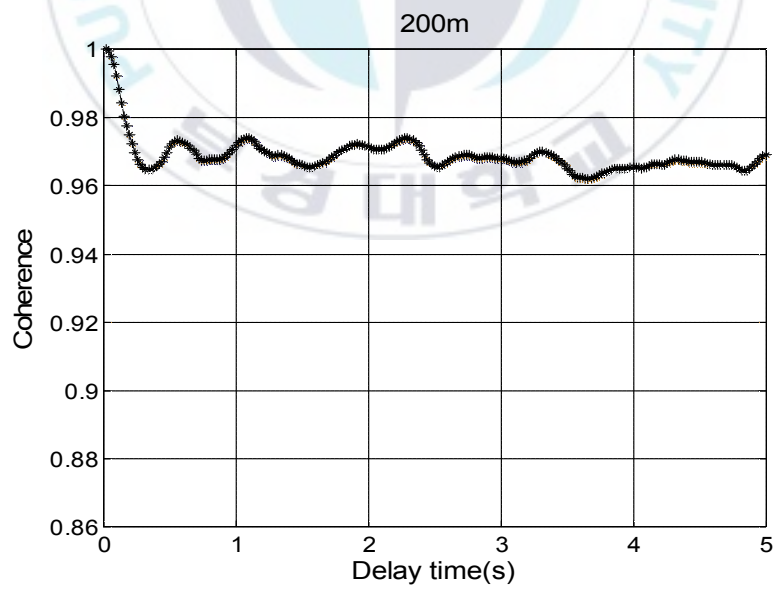
Table IV. Channel coherence bandwidths of four different Tx-Rx transmission ranges.

Tx-Rx range	Coherence bandwidth (-3 dB)	Coherence bandwidth (-6 dB)
100 m	60 Hz	600 Hz
200 m	400 Hz	1000 Hz
400 m	200 Hz	1200 Hz
800 m	200 Hz	1000 Hz

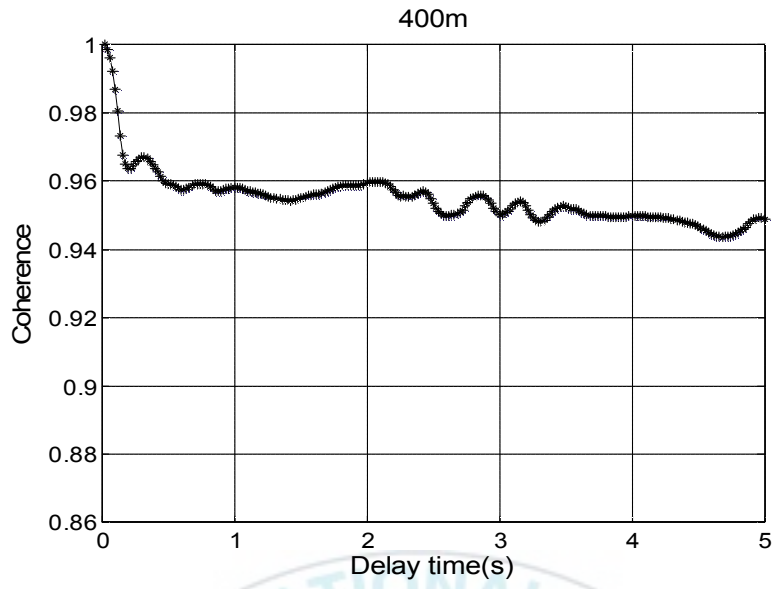
The LFM signal was also used to estimate the temporal coherence defined Eq. (12). The steps are as follows: First take one receiving signal of 10 ms LFM transmitting signal as the reference signal and then correlated with the late signals arriving at a later time. Second, take a next LFM receiving signal as the reference then one obtains another temporal coherence curve at different geo-time. Fig. 11 shows the average of all corresponding temporal coherence distribution for Tx-Rx ranges. One finds that the temporal coherence of 100 m drops to 0.88 in about 0.5 s but the temporal coherences of 200, 400 and 800 m show about 0.96. It is clear that Doppler spread is less than 1 for all TX-Rx ranges by the formula given in previous study[4]. Temporal coherence variation with time seems to follow well the surface fluctuation. The variation magnitude of 100 m range is larger than other ranges since relative motion of sea surface is greater than that of other ranges.



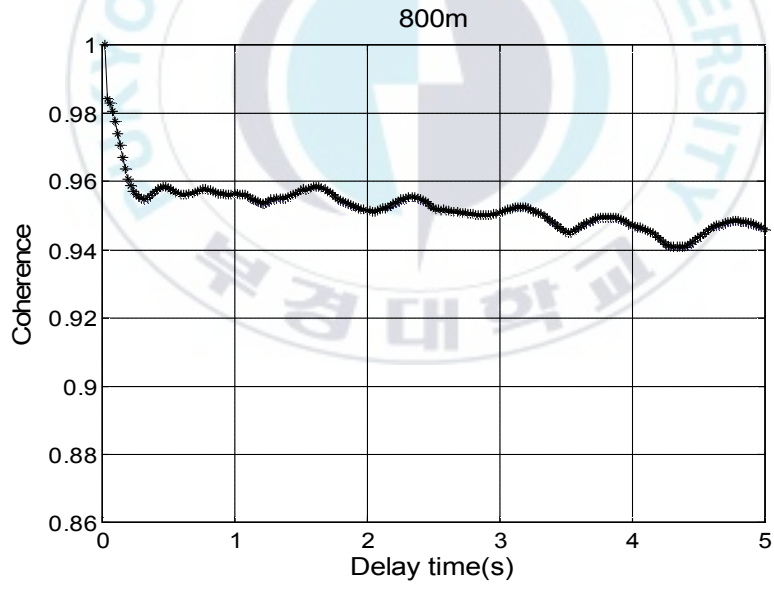
(a)



(b)



(c)



(d)

Fig. 11. Average temporal coherence for four Tx-Rx ranges: (a) 100 m; (b) 200 m; (c) 400 m; (d) 800 m.

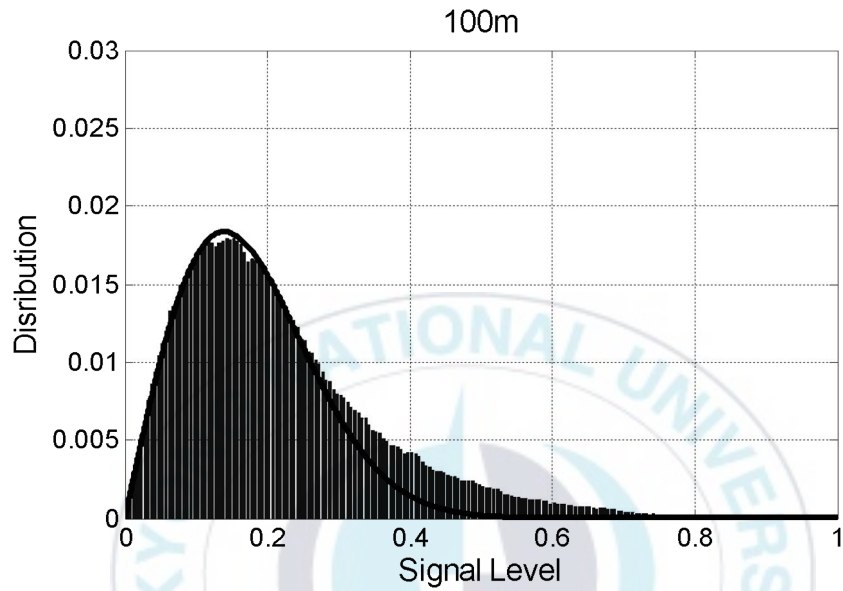
The statistics of amplitude envelope analyzed using PN signals. Fig. 12(a) shows probability densities of 16 kHz with 100 Hz bandwidth for four Tx-Rx ranges. 16 kHz is one of Ch3 frequencies of 4FSK for 1600 bps data rate. The probability densities are approximated as Rice distributions for 200, 400, and 800 m ranges but Rayleigh distribution for 100 m range. Fig. 12(b) shows probability densities of 12, 14, 16.8 and 18 kHz with 100 Hz bandwidth for Tx-Rx range of 100 m. These four frequencies are all activated at 1600 bps data rate in 100 m range. The probability densities are approximated as Rice distributions for 12 and 14 kHz but Rayleigh distributions for 16.8 and 18 kHz. Rice or Rayleigh distributions depend on range at fixed frequency and frequency at fixed range.

Rice or Rayleigh distributions depend on actually whether there are strong coherent multipath signals. In Fig. 9, there are at least two strong signals in each range (lumped or not). Therefore amplitude envelope of receiving signal $|h(\tau; t)|$ can be expressed as

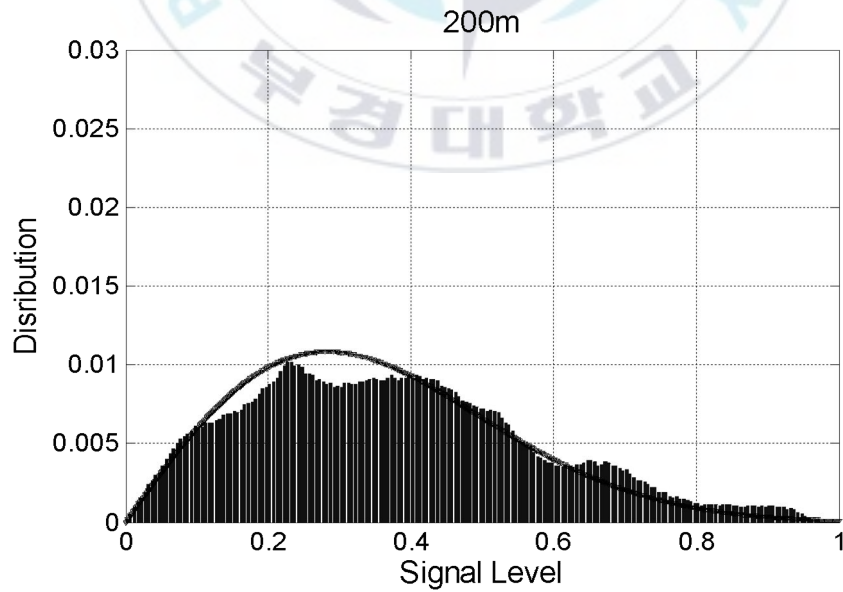
$$|h(\tau, t)| = \left| \alpha_1 + \alpha_2 e^{-j2\pi f_c \tau_2} + \alpha_3 e^{-j2\pi f_c \tau_3} + \beta(\tau, t) e^{-j2\pi f_c \tau} \right|. \quad (13)$$

Here it is assumed that there are three strong paths considering Fig. 9. If three discrete paths amplitude are similar to each other then overall level can be large or small by constructive or destructive addition of three terms in Eq. (13). Constructive or destructive addition determines whether fading statistics is Rice or Rayleigh

distribution, respectively. Since time delay τ_n to direct path depends on Tx-Rx range the envelope statistics depends on frequency in fixed range and range in fixed frequency. In Fig. 12, Rayleigh distribution is for destructive case and Rice distribution is for constructive case.



(i)



(ii)

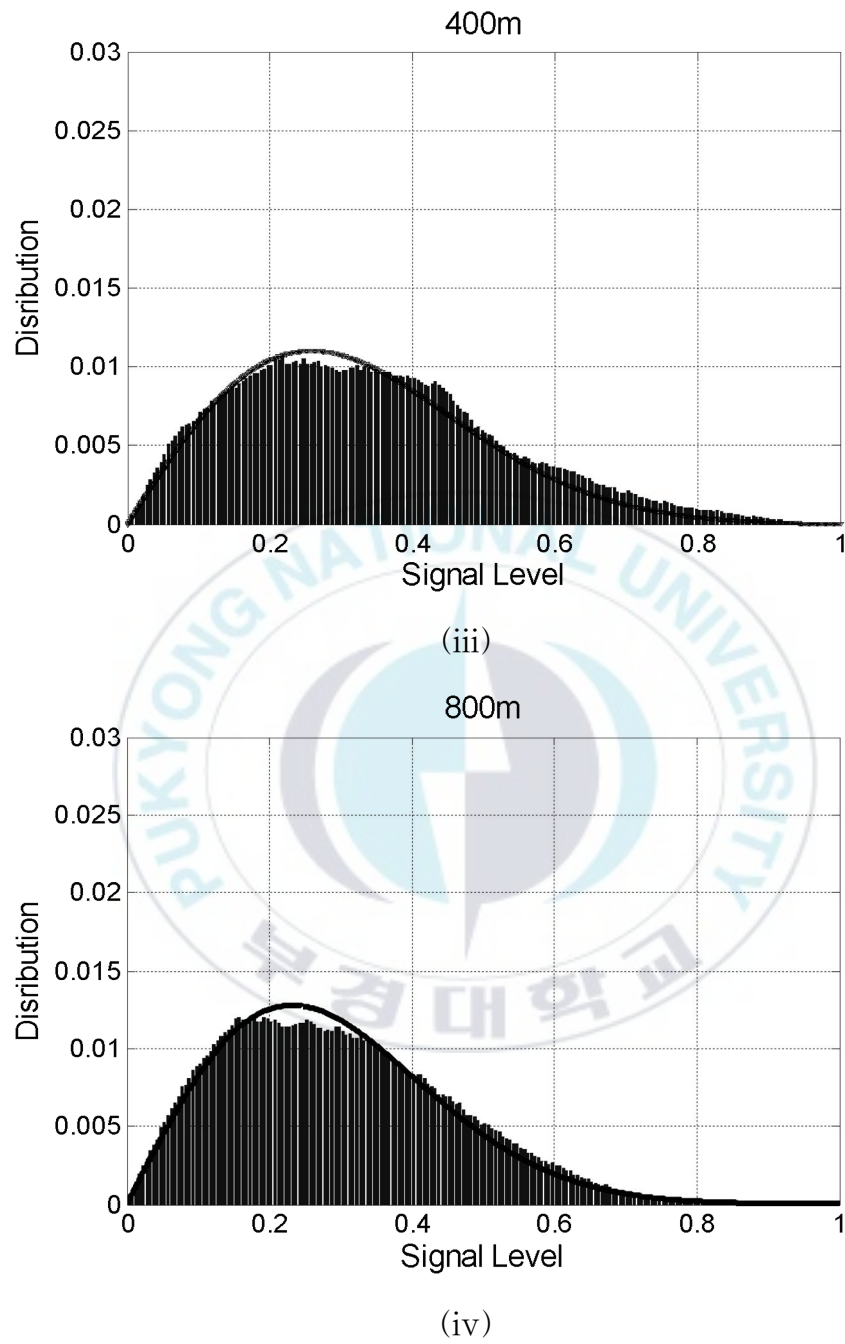
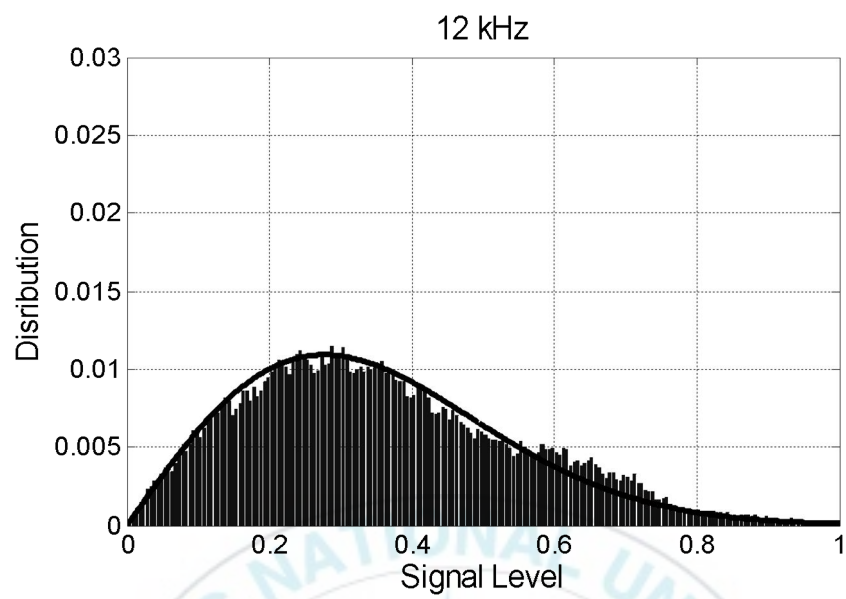
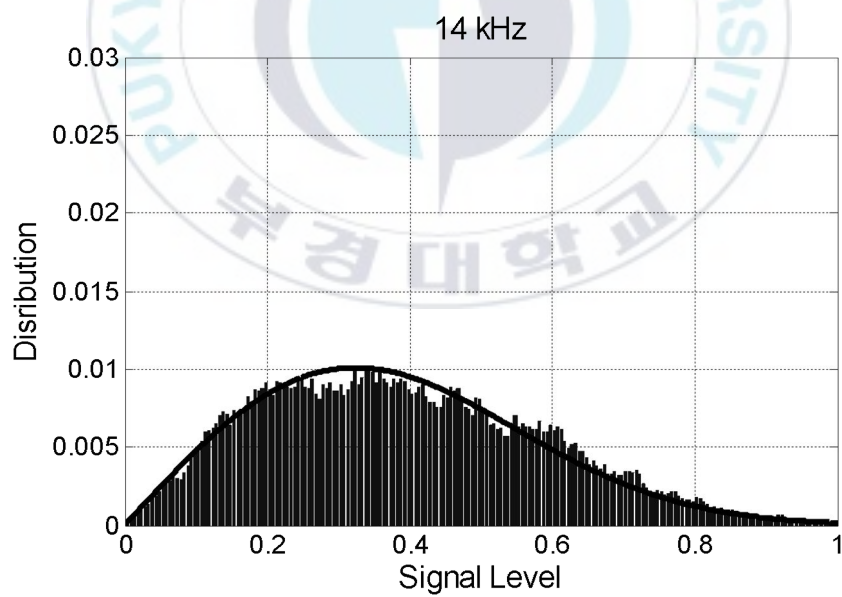


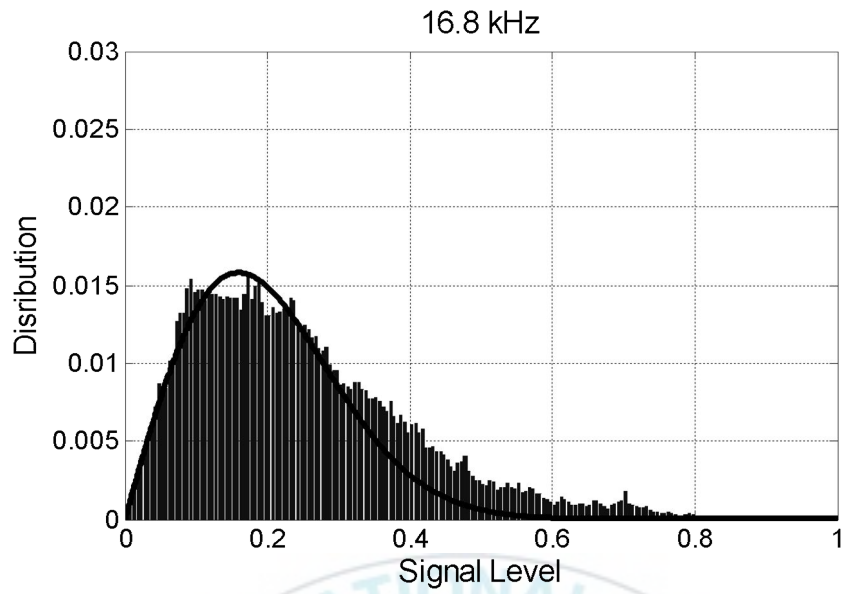
Fig. 12(a). Probability density of amplitude envelope for four Tx-Rx ranges at 16 kHz with 100 Hz bandwidth: (i) 100 m; (ii) 200 m; (iii) 400 m; (iv) 800 m.



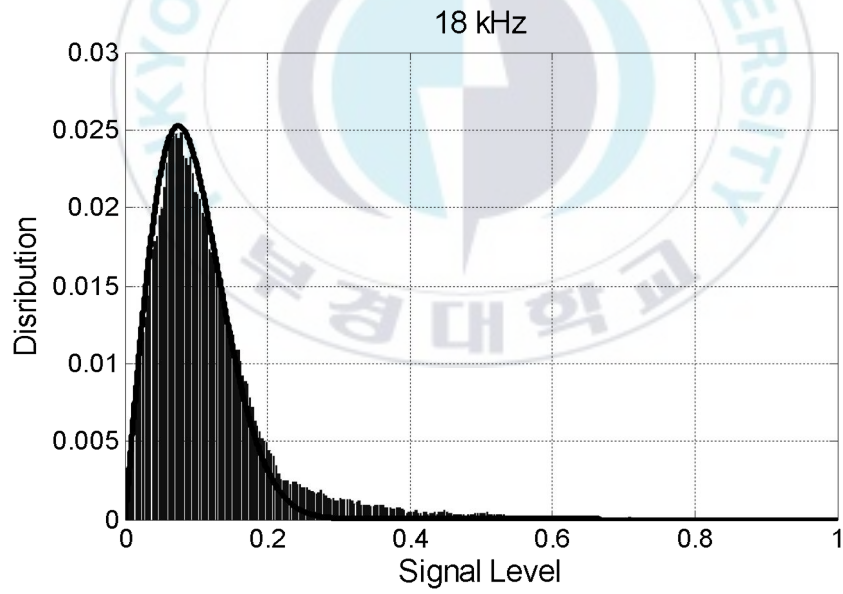
(i)



(ii)



(iii)

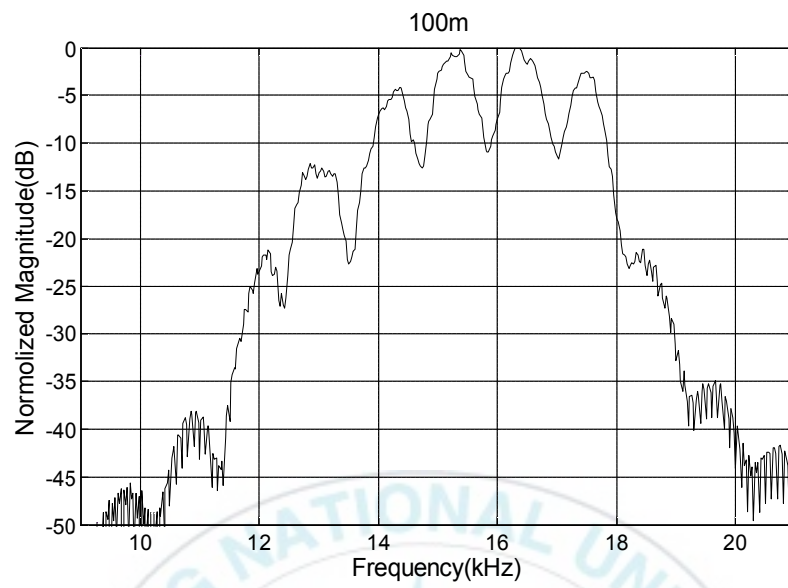


(iv)

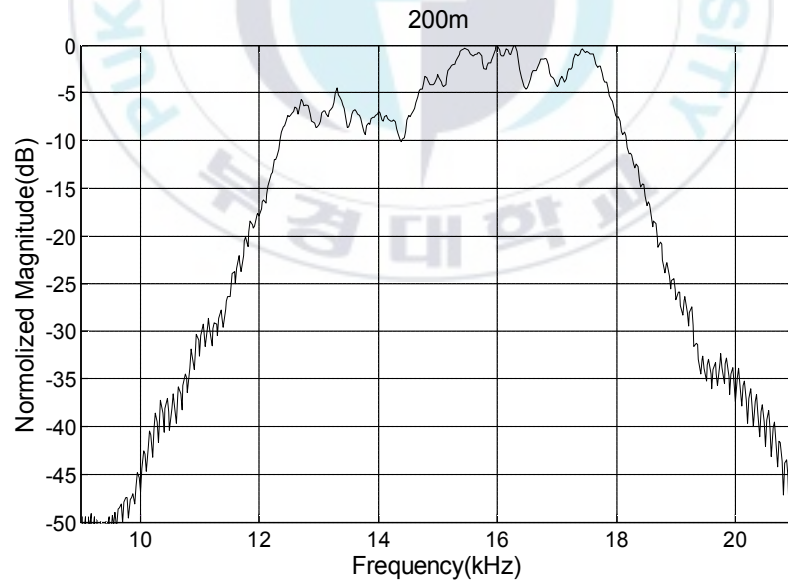
Fig. 12(b). Probability density of amplitude envelope of 12, 14, 16.8, and 18 kHz with 100 Hz for 100 m Tx-Rx range: (i) 12 kHz; (ii) 14 kHz; (iii) 16.8 kHz; (iv) 18 kHz.

Fig. 13 shows normalized receiving signal spectrum of LFM signal to confirm the fading statistics dependency on frequency and Tx-Rx range. The dips and the maxima in spectrum show destructive and constructive interference. Frequencies for dips and maxima give Rayleigh and Rice distributions, respectively.

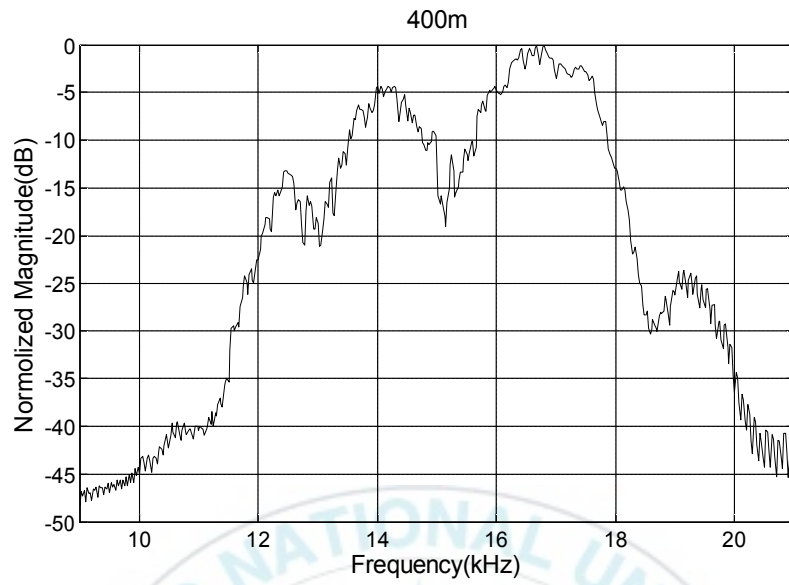
Fig. 14 shows error distributions of 4FSK signals based on frequency and geo-time for 100 and 800 m Tx-Rx ranges (· is original frequency; + is error frequency). In 100 m range, the errors mainly occur in 16.8 kHz frequency of Ch3 and 18 kHz and 19.2 kHz of Ch4, which the 16.8 and 18 kHz are approximated as Rayleigh distributions as shown in Fig. 12(b). In 800 m range the errors only occur in Ch2 and Ch4 which can be interpreted by dips of the spectrum shown in Fig. 13(d). Therefore, the MFSK system closely bounds up with the fading statistics which depends on the channel environmental factors and signal carrier frequency.



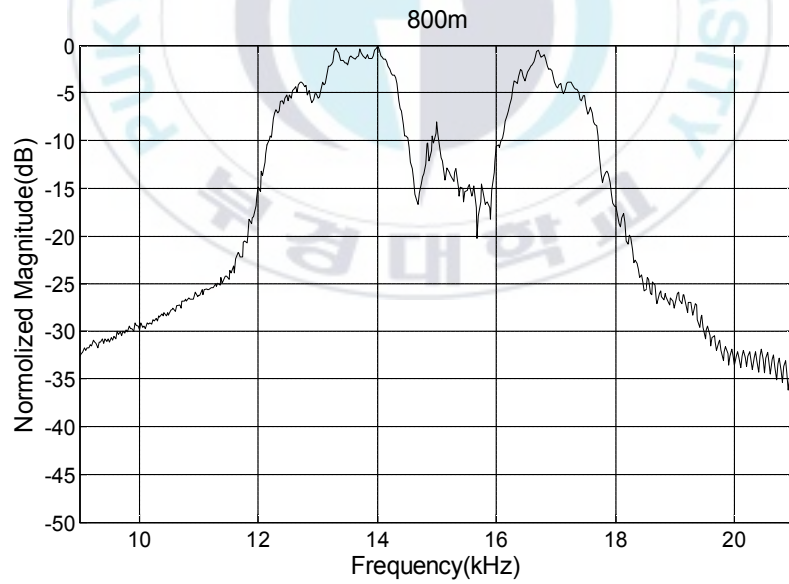
(a)



(b)

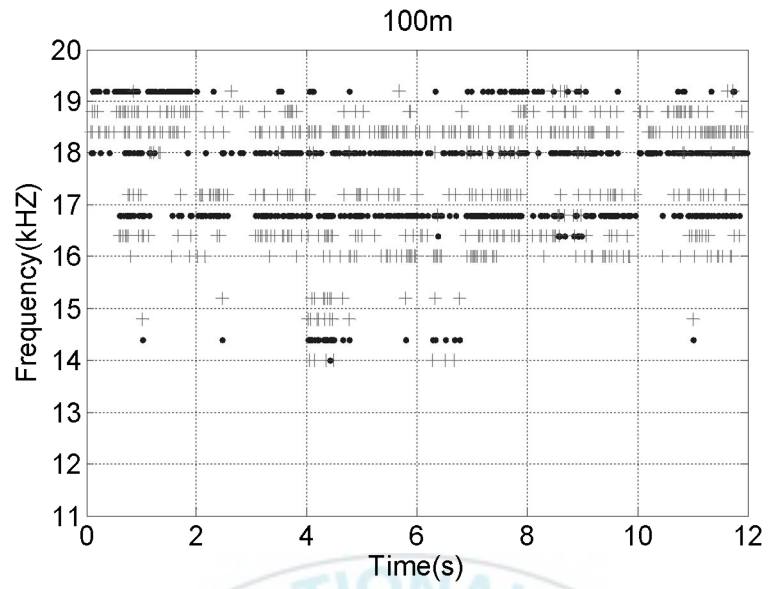


(c)

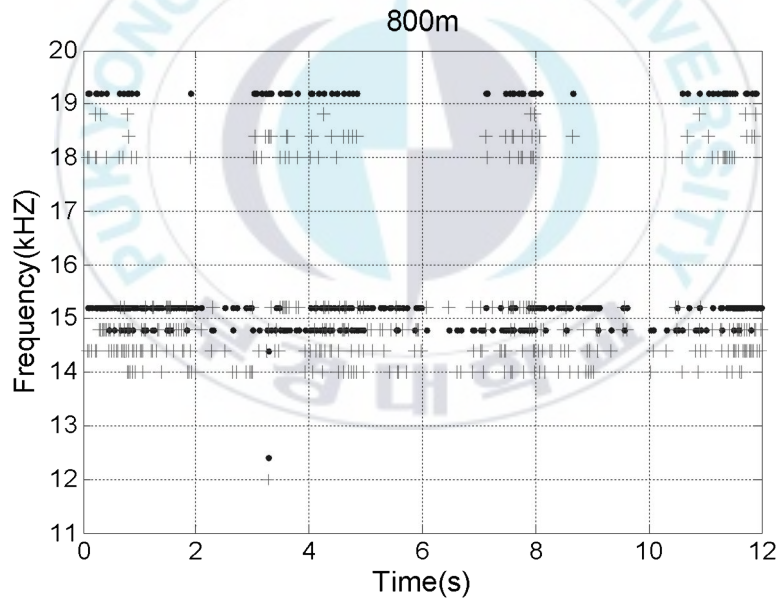


(d)

Fig. 13. Normalized receiving signal spectra of LFM signals for four Tx-Rx ranges: (a) 100 m; (b) 200 m; (c) 400 m; (d) 800 m.



(a)



(b)



Fig. 14. Error distributions of 4FSK signals based on frequency and geo-time for two Tx-Rx ranges: (a) 100 m; (b) 800 m. (· is original frequency; + is error frequency).

Table V shows the received images and BERs of four different data rates based on four Tx-Rx ranges. There are no errors in 200 and 400 m ranges. In both cases, -6 dB channel coherent bandwidth are 1000 and 1200 Hz as shown in Table IV. Maximum signal bandwidth for 1600 bps (400 sps) is 400 Hz. Therefore these two channels are frequency non selective. However, if there is destructive interference in any frequencies, corresponding frequency signal or channel may show Rayleigh fading resulting in increasing errors. It is interpreted that Rayleigh fading does not appear even if there are two dips in 400 m range as shown in Fig. 13.

For the 800 m range, there are not any errors in 200 and 400 bps (50 and 100 sps). In this case the channel is frequency non selective and Rice fading. As shown in Fig. 13, there are not any dips within 4FSK carrier frequency range from 12 kHz to 13.8 kHz as shown in Table II. For the 800 and 1600 bps rate 4FSK carrier frequency range extends to 19.2 kHz and there is wide range of dip between 14 and 16 kHz as shown in Fig. 13(d) which may cause Rayleigh fading and increases symbol error.

The worst case of error occurrence is 100 m range. The -6 dB channel coherent bandwidth is 600 Hz to be frequency non selective for given data rate in Table II. Therefore the error is caused mainly by Rayleigh fading due to destructive interference of discrete multipath. Since lower data rate give a narrower frequency range of 4FSK there is less chance of Rayleigh fading than higher data rate. Therefore BERs increase with data rate increase.

Table V. Received images and BERs.

	200 bps	400 bps	800 bps	1600 bps
100 m				
Error bits	130	138	532	856
BER	0.007	0.007	0.027	0.043
200 m				
Error bits	0	0	0	0
BER	0	0	0	0
400 m				
Error bits	0	0	0	0
BER	0	0	0	0
800 m				
Error bits	0	0	420	580
BER	0	0	0.021	0.029

6. Conclusions

The FSK system is known to be less sensitive to the fading channel and more robust to combat the effects of time-varying shallow water multipath channel. But the FSK signaling scheme has a disadvantage, which due to its low data rate. MFSK is adopted to increase a data rate but it requires wide range of frequency band to decrease channel efficiency in limited underwater channel. To quantify the effects of time varying shallow water channel on the performance of 4FSK system, channel impulse response, coherence bandwidth, temporal coherence and receiving signal envelope statistics are analyzed. LFM and PN signal with 12 to 19 kHz bandwidth are used and analyzed these parameters. Three distinct multipath signals at most are found in multipath intensity profiles. For four ranges from transmitter to receiver, temporal coherence is very high to give Doppler spread less than 1 Hz and its time variation follows well the sea state. The receiving signal envelope statistics depends on frequency and range due to the distinct strong multipath signals and their interference. It was found that this frequency and range dependency determines the envelope statistics or fading statistics to be Rayleigh or Rice distribution.

The BERs of received images using 4FSK system for four different data rates are examined for four Tx-Rx ranges. The channel is a frequency non selective slow fading. Because of fading dependency on frequency and range, the BER is strongly dependent on 4FSK carrier

frequency and Tx-Rx range.

In conclusion, the receiving signal amplitude varies with range from transmitter to receiver and therefore fading statistics also changes for a given sea roughness and frequency. Inherent factor of this fading change is a constructive or destructive interference. It is concluded that underwater acoustic channel fading statistics depends strongly on carrier frequency and Tx- Rx range if there are strong distinct multipath and scattering.



References

- [1] Milica Stojanovic, "Underwater Acoustic Communication", IEEE Electro International, Jun 1995.
- [2] Wen-Bin Yang, and T.C.Yang, "Characterization and Modeling of Underwater Acoustic communications channels for Frequency-Shift-Keying Signals", 1-4244-0115-1/06 MTS/IEEE OCEANS Boston Conference and Exhibition, 2006.
- [3] R.Galvin, and L.S.Wang, "Measured channel characteristics and the corresponding performance of an underwater acoustic communication system using parametric transduction", IEE Proc.-Rada, Sonar Navig., Vol. 147, No. 5, October 2000.
- [4] T. C. Yang, "Measurements of temporal coherence of sound transmissions through shallow water", J. Acoust. Soc. Am. 120 (5), November 2006, p.2595-2614.
- [5] Martin Siderius, Michael B. Porter, Paul Hursky, Vincent McDonald, and the KauaiEx Group, "Effects of ocean thermocline variability on noncoherent underwater acoustic communications", J. Acoust. Soc. Am. 121 (4), April 2007, p.1895-1908.
- [6] Y.L. Sun and Z.Han. "Cooperative Transmission for Underwater Acoustic Communications", IEEE International Conferences on Communication, May 2008.
- [7] E.M.Sozer, J.G.Proakis, and M.Stojanovic, "Underwater Acoustic Networks", IEEE Journal of Oceanic Engineering, 25(1), January 2000.
- [8] L.M.Brekhovskikh and Y.P.Lysonov, "Fundamentals of Ocean

Acoustic", Springer Verlag, Berlin, 1991.

[9] Erdal Epcacan, "Underwater Channel Modeling for Sonar Applications", Februray 2011.

[10] Sung-Hoon Byun, Sea-Moon Kim, Yong-Kon Lim, and Woojae Seong, "Time-varying Underwater Acoustic Channel Modeling for Moving Platform", MTS / IEEE-OES Conference, 0-933957-35-1, 2007.

[11] 樊昌信, 曹麗娜, "通信原理", 國防工業出版社, 第六版, 2010.

[12] Herman Medwin, and Clarence S. Clay, "Fundamentals of Acoustical Oceanography" (Academic Press, 1997), Chap.13.

[13] John G. Proakis, and Masoud Salehi, "Digital Communications" (McGraw- Hill, New York), 5th Edition, Chap.13.

[14] 박용완, 홍인기, 최정희, "이동통신공학", 생능출판사, 제2판, 2007.